BEILSTEIN JOURNAL OF NANOTECHNOLOGY

Ag_2WO_4 nanorods decorated with AgI nanoparticles: Novel and efficient visible-light-driven photocatalysts for the degradation of water pollutants

Shijie Li[*1], Shiwei Hu[1], Wei Jiang[1], Yanping Liu[2], Yu Liu[1], Yingtang Zhou[*1], Liuye Mo[1] and Jianshe Liu[3]

Full Research Paper

Open Access

Address:
[1]Key Laboratory of Health Risk Factors for Seafood of Zhejiang Province, Institute of Innovation & Application, Zhejiang Ocean University, Zhoushan, Zhejiang Province, 316022, China, [2]Department of Environmental Engineering, Zhejiang Ocean University, Zhoushan, Zhejiang Province, 316022, China, and [3]State Environmental Protection Engineering Center for Pollution Treatment and Control in Textile Industry, College of Environmental Science and Engineering, Donghua University, Shanghai 201620, China

Email:
Shijie Li[*] - lishijie@zjou.edu.cn; Yingtang Zhou[*] - zhouyingtang@zjou.edu.cn

* Corresponding author

Keywords:
AgI/Ag_2WO_4; nanocomposites; photocatalysis; visible light

Beilstein J. Nanotechnol. **2018,** *9,* 1308–1316.
doi:10.3762/bjnano.9.123

Received: 02 January 2018
Accepted: 29 March 2018
Published: 27 April 2018

This article is part of the Thematic Series "Energy conversion, storage and environmental remediation using nanomaterials".

Guest Editor: W.-J. Ong

Abstract

To develop efficient and stable visible-light-driven (VLD) photocatalysts for pollutant degradation, we synthesized novel heterojunction photocatalysts comprised of AgI nanoparticle-decorated Ag_2WO_4 nanorods via a facile method. Various characterization techniques, including XRD, SEM, TEM, EDX, and UV–vis DRS were used to investigate the morphology and optical properties of the as-prepared AgI/Ag_2WO_4 catalyst. With AgI acting as the cocatalyst, the resulting AgI/Ag_2WO_4 heterostructure shows excellent performance in degrading toxic, stable pollutants such as rhodamine B (RhB), methyl orange (MO) and *para*-chlorophenol (4-CP). The high performance is attributed to the enhanced visible-light absorption properties and the promoted separation efficiency of charge carriers through the formation of the heterojunction between AgI and Ag_2WO_4. Additionally, AgI/Ag_2WO_4 exhibits durable stability. The active species trapping experiment reveals that active species ($O_2^{\bullet-}$ and h^+) dominantly contribute to RhB degradation. The AgI/Ag_2WO_4 heterojunction photocatalyst characterized in this work holds great potential for remedying environmental issues due to its simple preparation method and excellent photocatalytic performance.

Introduction

The development of high-performance novel photocatalysts for the degradation of pollutants has received great interest due to the worsening of environmental pollution [1-11]. However, achieving high efficiency for photocatalytic conversion under natural sunlight irradiation is still a great challenge because many catalysts only respond to ultraviolet (UV) light [5,12]. Exploring photocatalysts that can be driven by visible light, which comprises 43% of solar energy, is important for practical application [13-20].

Silver-containing compounds such as AgI, Ag_2CrO_4, Ag_2O, Ag_3PO_4 etc., have proven to be efficient VLD photocatalysts [21-35]. Among these photocatalysts, Ag_2WO_4 presents good photocatalytic performance for dye degradation under light irradiation [30,31,36,37]. Unfortunately, due to its wide bandgap of about 3.1 eV, Ag_2WO_4 has limited photocatalytic activity under sunlight, which severely limits its application and illustrates the urgency for optimization of Ag_2WO_4 to overcome these disadvantages [38-42].

The integration of VLD components with wide bandgap semiconductors having well-matched energy bands has provided a new opportunity for the development of VLD photocatalysts [12]. As a consequence, some Ag_2WO_4-based composites containing VLD components such as Ag_2S/Ag_2WO_4 [40], C_3N_4/Ag_2WO_4 [39], $Bi_2MoO_6/Ag_2WO_4/Ag$ [42] etc., have been reported to show improved VLD performance in the degradation of pollutants. To the best of our knowledge, application of AgI/Ag_2WO_4 as a VLD photocatalyst for the degradation of toxic pollutants remains unreported.

In this study, to enhance the photocatalytic performance of Ag_2WO_4, AgI (possessing matched energy band levels) was chosen as a suitable component to combine with Ag_2WO_4, AgI/Ag_2WO_4 heterojunctions at different mole ratios. These heterojunctions were prepared via an in situ ion-exchange approach, utilizing Ag_2WO_4 nanorods as the Ag source. The as-prepared AgI/Ag_2WO_4 heterojunctions exhibited remarkably higher photocatalytic activity than pure Ag_2WO_4 toward the degradation of rhodamine B (RhB), methyl orange (MO) and *para*-chlorophenol (4-CP) under visible light. Based on a systematic characterization and study, a possible photocatalytic mechanism over AgI/Ag_2WO_4 was also elucidated in this work.

Results and Discussion

Preparation and characterization of catalysts

Ag_2WO_4 nanorods decorated with AgI nanoparticles were prepared via an in situ anion-exchange method. Ag_2WO_4 nanorods were first synthesized by mixing $AgNO_3$ and Na_2WO_4 aqueous solutions at room temperature [37]. Subsequently, AgI nanoparticles were readily anchored onto Ag_2WO_4 nanorods via an in situ anion-exchange between I^- in the solution and the lattice $W_2O_4^{2-}$ in Ag_2WO_4. The resulting catalysts were denoted as $0.1AgI/Ag_2WO_4$, $0.2AgI/Ag_2WO_4$, $0.3AgI/Ag_2WO_4$, and $0.4AgI/Ag_2WO_4$, respectively.

The XRD patterns of pure Ag_2WO_4, pure AgI, and AgI/Ag_2WO_4 heterojunctions are displayed in Figure 1. Pure Ag_2WO_4 is in its orthorhombic structure (JCPDS no. 70-1719) and exhibits several strong peaks at 30.3°, 31.8°, 33.1, 45.6°, 54.8° and 58.3°, which can be indexed to (002), (231), (400), (402), (361) and (333) diffraction planes, respectively [31,41]. The diffraction peaks of pure AgI match well with those of the standard hexagonal phase (JCPS no 29-1154) [43]. It can be seen that all the AgI/Ag_2WO_4 composites display both Ag_2WO_4 and AgI phases. Of note is that the diffraction peak intensity of AgI becomes stronger with increasing AgI content, confirming the formation of AgI/Ag_2WO_4 heterojunctions.

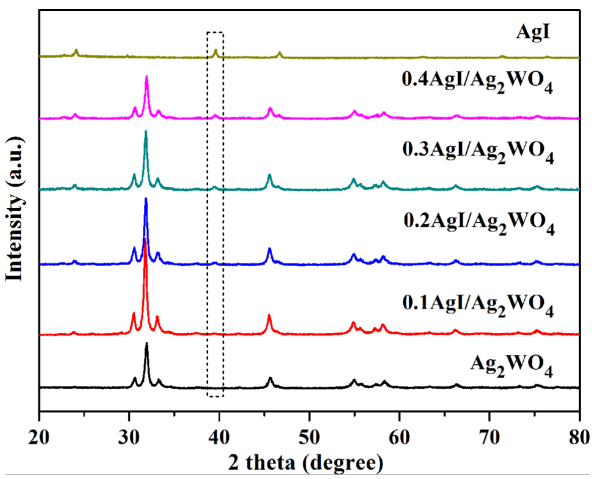

Figure 1: XRD patterns of Ag_2WO_4, AgI, $0.1AgI/Ag_2WO_4$, $0.2AgI/Ag_2WO_4$, $0.3AgI/Ag_2WO_4$, and $0.4AgI/Ag_2WO_4$.

Scanning electron microscopy (SEM) and transmission electron microscopy (TEM) were used to investigate the morphology and microstructure of AgI/Ag_2WO_4 heterojunctions (Figure 2). Figure 2a–d presents the SEM images of Ag_2WO_4 (Figure 2a,b) and the representative $0.3AgI/Ag_2WO_4$ (Figure 2c,d). It can be seen that bare Ag_2WO_4 consists of nanorods (length: 0.3–0.8 μm) with smooth surfaces (Figure 2a,b). After in situ anion-exchange between I^- and the lattice $W_2O_4^{2-}$, small AgI nanoparticles (diameter: 20–40 nm) are uniformly coated on the surface of Ag_2WO_4 nanorods, signifying the formation of the AgI/Ag_2WO_4 core–shell heterostructure. To more clearly observe the microstructure of the AgI/Ag_2WO_4 composite, the TEM and high-resolution TEM

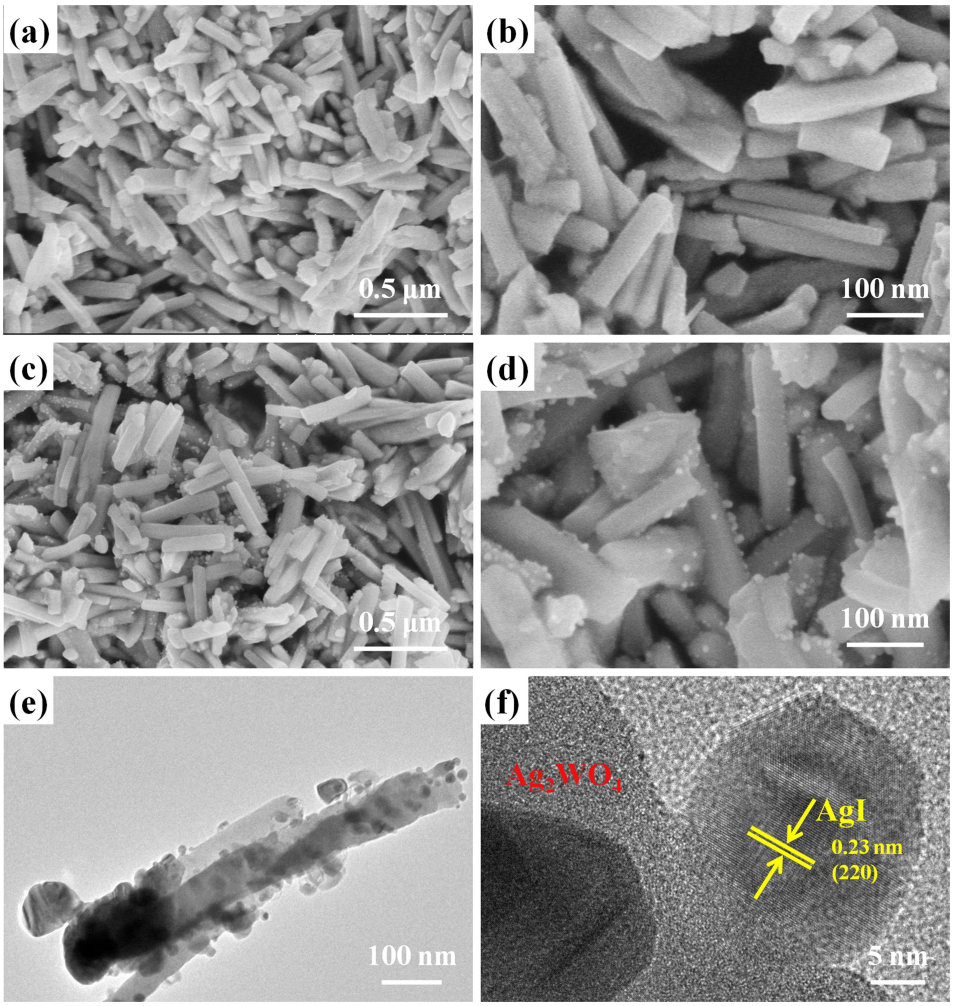

Figure 2: SEM (a, b) images of Ag_2WO_4; SEM (c, d), TEM (e), and HRTEM (f) images of 0.3AgI/Ag_2WO_4.

(HRTEM) images are shown in Figure 2e,f. It can be seen that many nanoparticles are deposited on the surface of the Ag_2WO_4 nanorods (Figure 2e). The HRTEM image (Figure 2f) shows that one set of lattice fringes can be observed. The lattice fringe of 0.23 nm matches well with the (220) plane of AgI. No lattice fringe correlated to Ag_2WO_4 can be distinguished, which is in accordance with the previous reports [40].

In addition, the composition of 0.3AgI/Ag_2WO_4 was further identified by energy-dispersive X-ray spectroscopy (EDX). As shown in Figure 3, 0.3AgI/Ag_2WO_4 is composed of Ag, I, W and O elements. The results further confirm the formation of the AgI/Ag_2WO_4 heterojunctions, thereby facilitating the charge transfer between them [12].

Subsequently, the optical properties of as-prepared photocatalysts were investigated by UV–vis diffuse reflectance spectroscopy (DRS) analysis (Figure 4). As indicated from Figure 4,

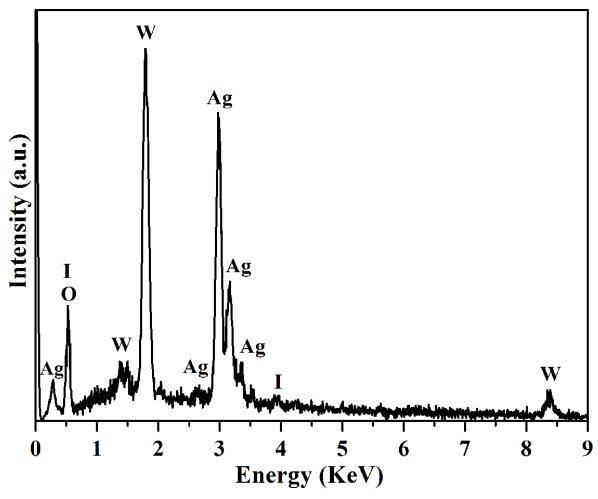

Figure 3: Energy-dispersive X-ray (EDX) spectrum of 0.3AgI/Ag_2WO_4.

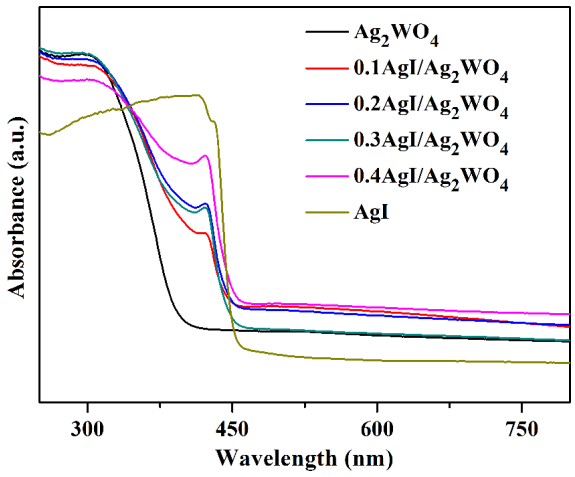

Figure 4: UV–vis diffuse reflectance spectra of Ag_2WO_4, AgI, 0.1AgI/Ag_2WO_4, 0.2AgI/Ag_2WO_4, 0.3AgI/Ag_2WO_4, and 0.4AgI/Ag_2WO_4.

pure Ag_2WO_4 has a clear absorption edge at about 400 nm [31], while AgI has a broader absorption band with the absorption edge located at around 460 nm [22]. For AgI/Ag_2WO_4 heterojunctions, a pronounced enhancement in visible-light absorption range is achieved when AgI content was progressively increased. This suggests that the introduction of AgI nanoparticles can optimize the light absorption capacity owing to the formation of a nanojunction between AgI and Ag_2WO_4. These facts indicate that AgI/Ag_2WO_4 heterojunctions can harvest more light and thus can be expected to be efficient VLD photocatalysts.

Photocatalytic performance

RhB, MO, and 4-CP, three types of toxic pollutants with stable chemical structures, were used to evaluate the activity of AgI/Ag_2WO_4 heterojunctions. Figure 5a shows the visible-light degradation results of RhB (10 mg L^{-1}) over as-prepared samples. Bare Ag_2WO_4 exhibits poor visible-light photocatalytic activity with an RhB degradation rate of 16.2% after 60 min irradiation due to the unsatisfactory visible-light absorption and fast recombination of photoinduced charge carriers [31,38,44,45]. After hybridization of AgI, all AgI/Ag_2WO_4 heterojunctions (0.1AgI/Ag_2WO_4, 0.2AgI/Ag_2WO_4, 0.3AgI/Ag_2WO_4, and 0.4AgI/Ag_2WO_4) show greatly improved photocatalytic activity compared with pure Ag_2WO_4, and their degradation efficiency (within 60 min of reaction) are 56.8%, 72.7%, 91.3% and 85.6%, respectively. Among these composites, 0.3AgI/Ag_2WO_4 shows the highest performance. Apparently, the introduction of a proper amount of AgI can markedly facilitate the separation of electron–hole pairs, leading to the marked photocatalytic activity, which is in accordance

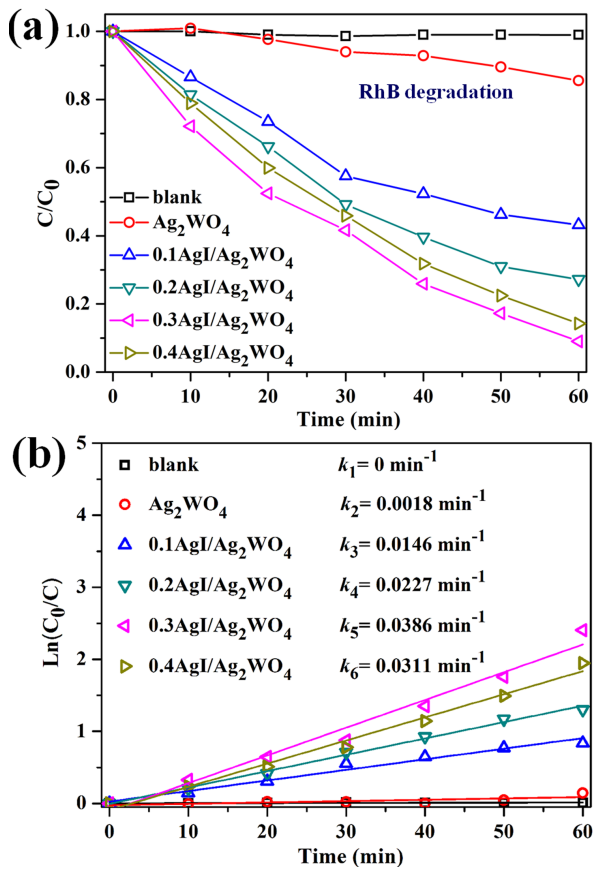

Figure 5: (a) The photocatalytic degradation and (b) degradation rate constants of RhB using different catalysts (10 mg) under visible light.

with previous reports. As the amount of AgI is further increased, the activity of 0.4AgI/Ag_2WO_4 decreases, indicating that excessive AgI is unfavorable for photocatalytic reaction. The possible reason is that a large amount of AgI particles having a larger diameter could interfere with the light absorption of reactive sites. It has also been found that the degradation process of RhB can be fitted well with the apparent first-order model (Figure 5b). As we can see, the k value for RhB decomposition over 0.3AgI/Ag_2WO_4 is about 0.0386 min^{-1}, which is much higher than those over other samples.

Besides RhB, MO (Figure 6a) and 4-CP (Figure S1, Supporting Information File 1) also could be efficiently degraded by 0.3AgI/Ag_2WO_4 under visible light, indicating the outstanding photocatalytic activity of 0.3AgI/Ag_2WO_4. In addition, the degradation rate constant of MO (Figure 6b) and 4-CP (Figure S1b, Supporting Information File 1) over catalysts were also calculated by the pseudo-first-order model. It is found that 0.3AgI/Ag_2WO_4 still achieves the highest apparent rate constant (0.0292 min^{-1} for MO degradation and 0.0129 min^{-1} for 4-CP degradation) among all these samples.

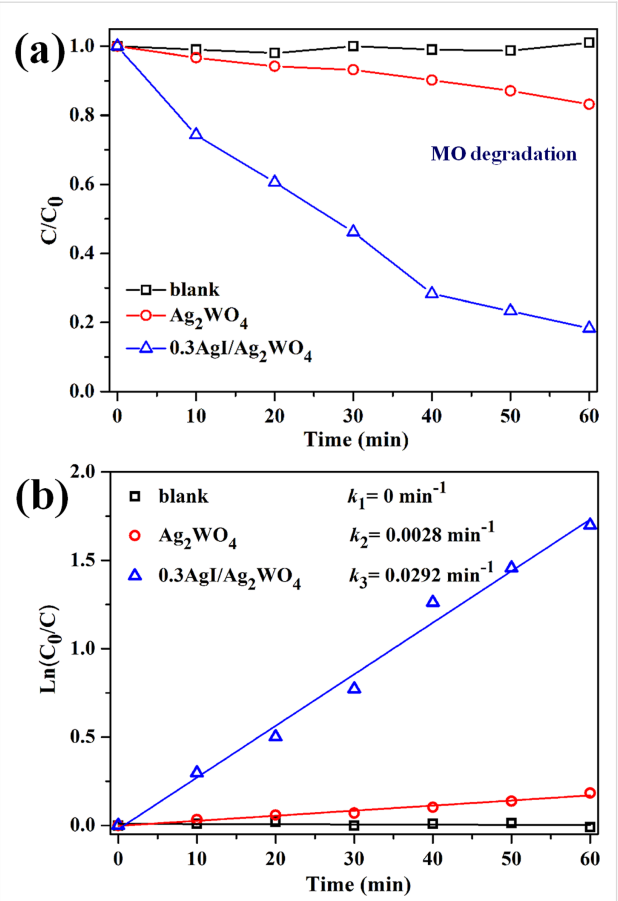

Figure 6: (a) The photocatalytic degradation and (b) degradation rate constants of MO (100 mL, 5 mg L^{-1}) using the catalysts (10 mg).

The mineralization of organic pollutants is crucial for pollutant treatment [46]. Thus, the total organic carbon (TOC) removal efficiency of RhB over $0.3AgI/Ag_2WO_4$ was examined (Figure 7). After 360 min of reaction, the TOC removal efficiency reached 67.2%, signifying that $0.3AgI/Ag_2WO_4$ can effectively mineralize RhB.

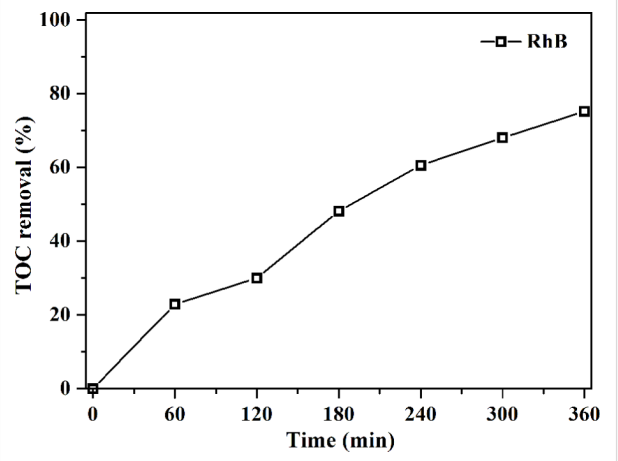

Figure 7: Total organic carbon (TOC) removal during the photocatalytic degradation of RhB in the presence of $0.3AgI/Ag_2WO_4$.

The operational lifetime of the photocatalysts is crucial for practical application [47]. To reveal the durability of $0.3AgI/Ag_2WO_4$, the cycling photocatalytic degradation of RhB was performed. As shown in Figure 8a, no apparent activity decrease was observed after five successive runs, demonstrating the good stability of the catalyst. Furthermore, the XRD pattern of the used $0.3AgI/Ag_2WO_4$ is similar to that of the fresh one (Figure 8b). These facts suggest that $0.3AgI/Ag_2WO_4$ possesses long-term stability for photocatalytic reaction.

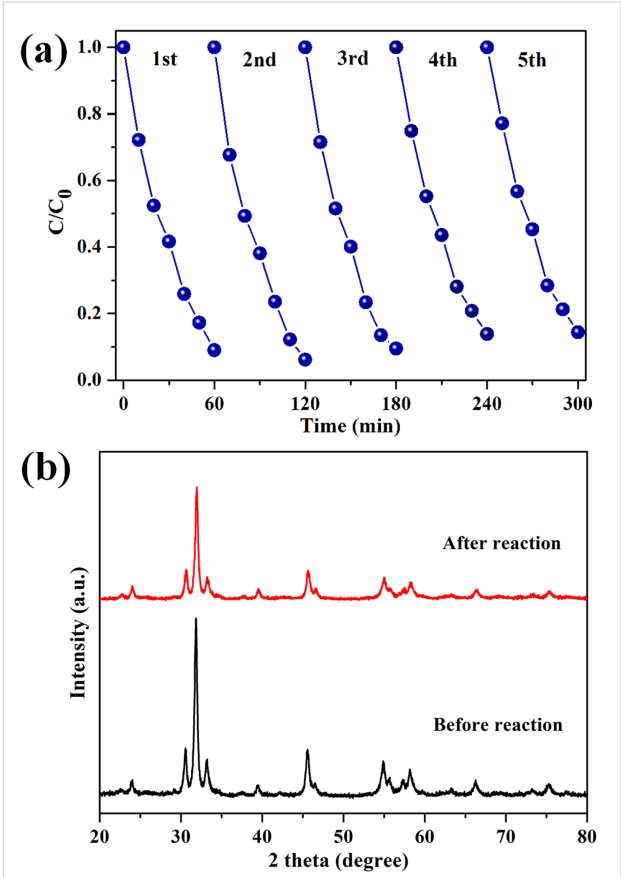

Figure 8: (a) The cycled photocatalytic degradation of RhB over $0.3AgI/Ag_2WO_4$; (b) XRD patterns of the fresh and used $0.3AgI/Ag_2WO_4$.

Photocatalytic mechanism

To elucidate the degradation mechanism, active-species trapping tests were performed during RhB degradation over $0.3AgI/Ag_2WO_4$ (Figure 9) [13,48]. Figure 9 shows the effects of various trapping agents on the RhB degradation efficiency under visible-light irradiation. When IPA was introduced, the RhB degradation efficiency slightly reduced from 91.3 % to 70.7%, suggesting that very little •OH was involved in the reac-

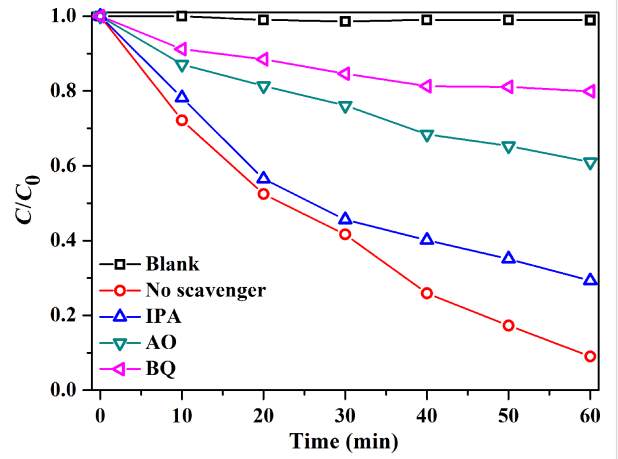

Figure 9: Active-species trapping tests over 0.3AgI/Ag_2WO_4.

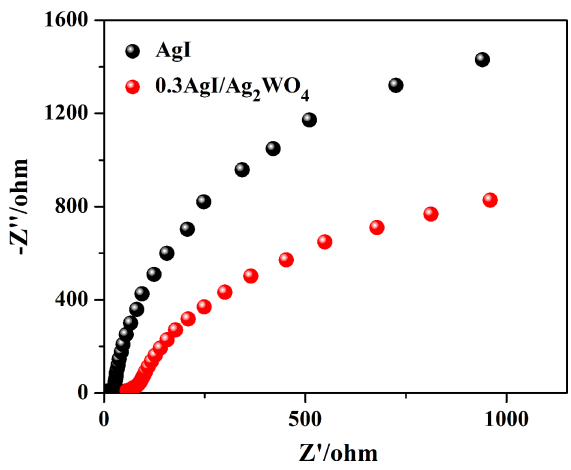

Figure 10: Electrochemical impedance spectroscopy (EIS) Nyquist plots of AgI and 0.3AgI/Ag_2WO_4.

tion. However, when benzoquinone (a superoxide radical ($•O_2^-$) scavenger) or ammonium oxalate (a hole radical (h^+) scavenger) was introduced, the degradation rate of RhB was severely depressed. That is, $•O^{2-}$, •OH, and h^+ were generated in the 0.3AgI/Ag_2WO_4 mediated degradation system, but $•O^{2-}$ and h^+ played a more crucial role in RhB degradation.

Electrochemical impedance spectroscopy (EIS) measurement was applied to study the charge transport and separation [49]. A smaller arc radius commonly signifies a higher charge transport rate. As displayed in Figure 10, the arc radius of 0.3AgI/Ag_2WO_4 is smaller than that of AgI, suggesting that 0.3AgI/Ag_2WO_4 holds a higher charge transfer rate and a more effective separation of charge carriers.

On the basis of the above discussion, the excellent photocatalytic activity of AgI/Ag_2WO_4 is concluded to be due to the broadening of the photo-absorption range from the ultraviolet to the visible light range (Figure 4) and the formation of a heterojunction between AgI and Ag_2WO_4. The matched band alignments lead to a fascinating separation and transfer of the photo-generated electrons and holes (Figure 11) [50-52]. A heterostructure is well constructed after the in situ growth of AgI on Ag_2WO_4. Under visible light irradiation, AgI is excited to produce electrons and holes. Given the negative potential of conduction band (CB) of AgI to that of Ag_2WO_4, electrons tend to migrate from the CB of AgI to that of Ag_2WO_4, whereby the separation rate of electron–hole pairs is boosted. Consequently, the accu-

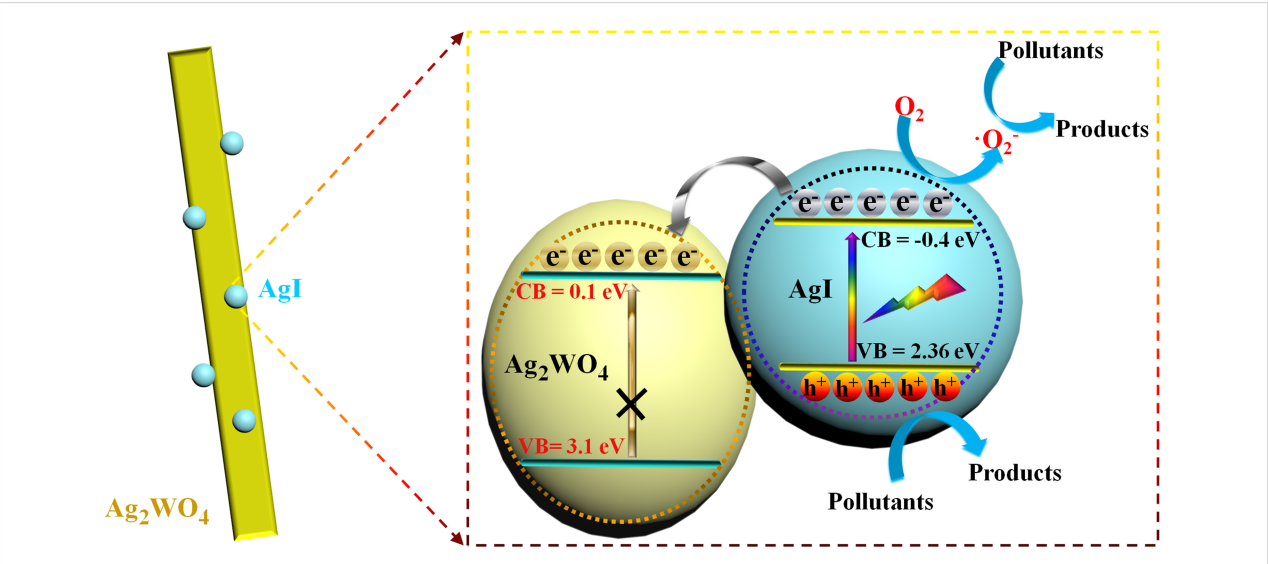

Figure 11: Schematic diagram of electron–hole pair separation and the possible reaction mechanism over the AgI/Ag_2WO_4 heterojunction under visible-light irradiation.

mulated electrons in the CB of AgI (and more holes left behind in the valence band (VB)) could readily attack the pollutant molecules, resulting in the remarkable photocatalytic performance of AgI/Ag_2WO_4.

Conclusion

In summary, a novel heterojunction photocatalyst comprised of AgI nanoparticle-decorated Ag_2WO_4 nanorods exhibiting remarkable photocatalytic performance has been prepared via a facile method. This resulting AgI/Ag_2WO_4 catalyst exhibits exceptionally high and stable photocatalytic activity for the degradation of RhB, MO and 4-CP due to its extended light absorption range and the formation of a heterojunction between AgI and Ag_2WO_4. This work not only offers a high-efficiency AgI/Ag_2WO_4 heterojunction photocatalyst, but also provides new inspiration for the development of visible-light-driven Ag-based heterojunction photocatalysts.

Experimental

Photocatalyst synthesis

All reagents were purchased from Shanghai Sinopharm Chemical Reagent Ltd. and used as received.

Ag_2WO_4 nanorods were prepared according to a previous report [41]. Briefly, $AgNO_3$ (0.01 mol L^{-1}, 100 mL) and Na_2WO_4 (0.005 mol L^{-1}, 100 mL) aqueous solutions were first prepared. Then, the $AgNO_3$ aqueous solution was slowly poured into Na_2WO_4 aqueous solution and incubated at room temperature for 12 h in the dark. Finally, the white precipitate was collected, washed successively with distilled water, and dried in vacuum at 60 °C for 12 h.

The AgI/Ag_2WO_4 nanorods were prepared by an in situ anion-exchange reaction of Ag_2WO_4 nanorods in KI aqueous solution at a temperature of 60 °C in the dark. In a typical reaction, KI (0.1 mmol, 0.2 mmol, 0.3 mmol, 0.4 mmol) was dissolved separately in 60 mL distilled water and stirred to obtain a clear solution. Then, the as-prepared Ag_2WO_4 nanorods (1 mmol) were dispersed respectively in each of the above solutions at 60 °C under stirring for 5 h. After reaction, the products with different amounts of KI (0.1 mmol, 0.2 mmol, 0.3 mmol, 0.4 mmol) were collected, washed, and finally dried in vacuum at 60 °C for 12 h. The products prepared with different amounts of KI (0.1 mmol, 0.2 mmol, 0.3 mmol, 0.4 mmol) were denoted as 0.1AgI/Ag_2WO_4, 0.2AgI/Ag_2WO_4, 0.3AgI/Ag_2WO_4, and 0.4AgI/Ag_2WO_4, respectively.

Characterization

The crystalline structure of the samples was studied by using a Bruker D8 Advance X-ray diffractometer (XRD). The images of the morphological structure were observed by a field emission scanning electron microscope (FE-SEM, Hitachi S–4800) and a high-resolution transmission electron microscope (HRTEM, JEOL JEM–2010F). Energy-dispersive X-ray (EDX) spectroscopy coupled with SEM was employed to identify the chemical composition of the sample. UV–vis diffuse reflectance spectra (UV–vis DRS) were recorded on an UV–vis spectrophotometer (Shimadzu, UV-2600).

Photocatalytic tests

The photocatalytic activity of the as-prepared samples was evaluated by the removal of RhB, MO or 4-CP under visible-light irradiation. A 300 W Xe lamp with a cut-off filter ($\lambda > 400$ nm) was used as the light source during the reaction. In each experiment, 10 mg of catalyst was dispersed in RhB (100 mL, 10 mg L^{-1}), MO (100 mL, 5 mg L^{-1}) or 4-CP (100 mL, 5 mg L^{-1}) aqueous solution. Before light illumination, the suspensions were first magnetically stirred in the dark for 1 hour. Then 2 mL of the suspension was collected and the light was switched on. With the light on and under magnetic stirring, 2 mL of the suspension was sampled at given time intervals. All suspensions were centrifuged to remove the catalyst particles. The RhB and MO concentrations were monitored by a UV-2600 spectrometer. The 4-CP concentrations were monitored by high-performance liquid chromatography (HPLC, Agilent 110 series).

The total organic carbon (TOC) experiment was carried out by dispersing 100 mg of 0.3AgI/Ag_2WO_4 in RhB (50 mg L^{-1}, 100 mL) solution. During the reaction, a 10 mL suspension was sampled every hour and monitored by a TOC analyzer (Shimadzu TOC-VCPH).

Radical trapping experiments were conducted by introducing diverse scavengers (1 mM ammonium oxalate, 1 mM *p*-benzoquinone or 1 mM isopropanol) into the RhB (100 mL, 10 mg L^{-1}) solution.

Supporting Information

Supporting Information File 1

Additional figure.
Degradation of *para*-chlorophenol (4-CP) by 0.3AgI/Ag2WO4 under visible light and the degradation rate constants 4-CP.
[https://www.beilstein-journals.org/bjnano/content/supplementary/2190-4286-9-123-S1.tif]

Acknowledgements

This work has been financially supported by the National Natural Science Foundation of China (51708504 and

31501573), the Public Projects of Zhejiang Province (2017C32079 and LGN18E080003), the Science and Technology project of Zhoushan (2017C41006, 2016C41012, 2015C21014, 2015C21013) and the Research Startup Foundation of Zhejiang Ocean University (12215090117).

References

1. Li, S.; Zhang, L.; Wang, H.; Chen, Z.; Hu, J.; Xu, K.; Liu, J. *Sci. Rep.* **2014,** *4,* 3978. doi:10.1038/srep03978
2. Jing, P.; Lan, W.; Su, Q.; Xie, E. *Beilstein J. Nanotechnol.* **2015,** *6,* 1281–1286. doi:10.3762/bjnano.6.132
3. Zhang, G.; Liu, G.; Wang, L.; Irvine, J. T. S. *Chem. Soc. Rev.* **2016,** *45,* 5951–5984. doi:10.1039/c5cs00769k
4. Zhang, G.; Lan, Z.-A.; Wang, X. *Angew. Chem., Int. Ed.* **2016,** *55,* 15712–15727. doi:10.1002/anie.201607375
5. Ong, W.-J.; Tan, L.-L.; Ng, Y. H.; Yong, S.-T.; Chai, S.-P. *Chem. Rev.* **2016,** *116,* 7159–7329. doi:10.1021/acs.chemrev.6b00075
6. Han, W.; Li, Z.; Li, Y.; Fan, X.; Zhang, F.; Zhang, G.; Peng, W. *Front. Chem. (Lausanne, Switz.)* **2017,** *5,* 84. doi:10.3389/fchem.2017.00084
7. Ong, W.-J. *Front. Mater.* **2017,** *4,* 11. doi:10.3389/fmats.2017.00011
8. Kumar, S.; Kumar, A.; Bahuguna, A.; Sharma, V.; Krishnan, V. *Beilstein J. Nanotechnol.* **2017,** *8,* 1571–1600. doi:10.3762/bjnano.8.159
9. Huang, X.; Wang, J.; Li, T.; Wang, J.; Xu, M.; Yu, W.; Abed, A. E.; Zhang, X. *Beilstein J. Nanotechnol.* **2018,** *9,* 30–41. doi:10.3762/bjnano.9.5
10. Chen, X.; Li, N.; Kong, Z.; Ong, W.-J.; Zhao, X. *Mater. Horiz.* **2018,** *5,* 9–27. doi:10.1039/C7MH00557A
11. Zeng, S.; Kar, P.; Thakur, U. K.; Shankar, K. *Nanotechnology* **2018,** *29,* 052001. doi:10.1088/1361-6528/aa9fb1
12. Wang, H.; Zhang, L.; Chen, Z.; Hu, J.; Li, S.; Wang, Z.; Liu, J.; Wang, X. *Chem. Soc. Rev.* **2014,** *43,* 5234–5244. doi:10.1039/C4CS00126E
13. Li, S.; Shen, X.; Liu, J.; Zhang, L. *Environ. Sci.: Nano* **2017,** *4,* 1155–1167. doi:10.1039/c6en00706f
14. Li, S.; Hu, S.; Zhang, J.; Jiang, W.; Liu, J. *J. Colloid Interface Sci.* **2017,** *497,* 93–101. doi:10.1016/j.jcis.2017.02.069
15. Zhang, L.; Zhang, Q.; Xie, H.; Guo, J.; Lyu, H.; Li, Y.; Sun, Z.; Wang, H.; Guo, Z. *Appl. Catal., B* **2017,** *201,* 470–478. doi:10.1016/j.apcatb.2016.08.056
16. Laatar, F.; Moussa, H.; Alem, H.; Balan, L.; Girot, E.; Medjahdi, G.; Ezzaouia, H.; Schneider, R. *Beilstein J. Nanotechnol.* **2017,** *8,* 2741–2752. doi:10.3762/bjnano.8.273
17. Chen, C.; Ma, W.; Zhao, J. *Chem. Soc. Rev.* **2010,** *39,* 4206–4219. doi:10.1039/b921692h
18. Moniz, S. J. A.; Shevlin, S. A.; Martin, D. J.; Guo, Z.-X.; Tang, J. *Energy Environ. Sci.* **2015,** *8,* 731–759. doi:10.1039/C4EE03271C
19. Zhang, G.; Li, G.; Lan, Z.-A.; Lin, L.; Savateev, A.; Heil, T.; Zafeiratos, S.; Wang, X.; Antonietti, M. *Angew. Chem., Int. Ed.* **2017,** *129,* 13630–13634. doi:10.1002/ange.201706870
20. Zhang, G.; Lan, Z.-A.; Wang, X. *Chem. Sci.* **2017,** *8,* 5261–5274. doi:10.1039/C7SC01747B
21. Martin, D. J.; Liu, G.; Moniz, S. J. A.; Bi, Y.; Beale, A. M.; Ye, J.; Tang, J. *Chem. Soc. Rev.* **2015,** *44,* 7808–7828. doi:10.1039/C5CS00380F
22. Wang, X.; Yang, J.; Ma, S.; Zhao, D.; Dai, J.; Zhang, D. *Catal. Sci. Technol.* **2016,** *6,* 243–253. doi:10.1039/C5CY00787A
23. Liu, B.; Li, X.; Zhao, Q.; Ke, J.; Tadé, M.; Liu, S. *Appl. Catal., B* **2016,** *185,* 1–10. doi:10.1016/j.apcatb.2015.12.003
24. Yang, S.-F.; Niu, C.-G.; Huang, D.-W.; Zhang, H.; Liang, C.; Zeng, G.-M. *Environ. Sci.: Nano* **2017,** *4,* 585–595. doi:10.1039/C6EN00597G
25. Wang, X.; Li, S.; Yu, H.; Yu, J.; Liu, S. *Chem. – Eur. J.* **2011,** *17,* 7777–7780. doi:10.1002/chem.201101032
26. Xu, D.; Cheng, B.; Cao, S.; Yu, J. *Appl. Catal., B* **2015,** *164,* 380–388. doi:10.1016/j.apcatb.2014.09.051
27. Yu, C.; Li, G.; Kumar, S.; Yang, K.; Jin, R. *Adv. Mater.* **2014,** *26,* 892–898. doi:10.1002/adma.201304173
28. Jiao, Z.; Zhang, Y.; Yu, H.; Lu, G.; Ye, J.; Bi, Y. *Chem. Commun.* **2013,** *49,* 636–638. doi:10.1039/C2CC37324F
29. Zhu, X.; Wang, P.; Li, M.; Zhang, Q.; Rozhkova, E. A.; Qin, X.; Zhang, X.; Dai, Y.; Wang, Z.; Huang, B. *Catal. Sci. Technol.* **2017,** *7,* 2318–2324. doi:10.1039/C7CY00393E
30. Wang, X.; Fu, C.; Wang, P.; Yu, H.; Yu, J. *Nanotechnology* **2013,** *24,* 165602. doi:10.1088/0957-4484/24/16/165602
31. Xu, D.; Cheng, B.; Zhang, J.; Wang, W.; Yu, J.; Ho, W. *J. Mater. Chem. A* **2015,** *3,* 20153–20166. doi:10.1039/C5TA05248C
32. Li, S.; Hu, S.; Jiang, W.; Liu, Y.; Liu, J.; Wang, Z. *Mol. Catal.* **2017,** *435,* 135–143. doi:10.1016/j.mcat.2017.03.027
33. Li, J.; Yu, C.; Zheng, C.; Etogo, A.; Xie, Y.; Zhong, Y.; Hu, Y. *Mater. Res. Bull.* **2015,** *61,* 315–320. doi:10.1016/j.materresbull.2014.10.018
34. Ong, W.-J.; Putri, L. K.; Tan, L.-L.; Chai, S.-P.; Yong, S.-T. *Appl. Catal., B* **2016,** *180,* 530–543. doi:10.1016/j.apcatb.2015.06.053
35. Tang, H.; Fu, Y.; Chang, S.; Xie, S.; Tang, G. *Chin. J. Catal.* **2017,** *38,* 337–347. doi:10.1016/S1872-2067(16)62570-6
36. Dutta, D. P.; Singh, A.; Ballal, A.; Tyagi, A. K. *Eur. J. Inorg. Chem.* **2014,** *2014,* 5724–5732. doi:10.1002/ejic.201402612
37. Chen, H.; Xu, Y. *Appl. Surf. Sci.* **2014,** *319,* 319–323. doi:10.1016/j.apsusc.2014.05.115
38. Pirhashemi, M.; Habibi-Yangjeh, A. *J. Colloid Interface Sci.* **2017,** *491,* 216–229. doi:10.1016/j.jcis.2016.12.044
39. Li, Y.; Jin, R.; Fang, X.; Yang, Y.; Yang, M.; Liu, X.; Xing, Y.; Song, S. *J. Hazard. Mater.* **2016,** *313,* 219–228. doi:10.1016/j.jhazmat.2016.04.011
40. Wang, X.; Zhan, S.; Wang, Y.; Wang, P.; Yu, H.; Yu, J.; Hu, C. *J. Colloid Interface Sci.* **2014,** *422,* 30–37. doi:10.1016/j.jcis.2014.02.009
41. Wang, X.; Li, S.; Yu, H.; Yu, J. *J. Mol. Catal. A: Chem.* **2011,** *334,* 52–59. doi:10.1016/j.molcata.2010.10.022
42. Lv, J.; Dai, K.; Zhang, J.; Lu, L.; Liang, C.; Geng, L.; Wang, Z.; Yuan, G.; Zhu, G. *Appl. Surf. Sci.* **2017,** *391,* 507–515. doi:10.1016/j.apsusc.2016.05.001
43. Chen, J.; Li, S.; Hu, S.; Jiang, W. *Mater. Lett.* **2017,** *191,* 123–127. doi:10.1016/j.matlet.2016.12.096
44. Liu, X.; Hu, J.; Li, J.; Hu, Y.; Shao, Y.; Yang, H.; Tong, G.; Qian, H. *Mater. Lett.* **2013,** *91,* 129–132. doi:10.1016/j.matlet.2012.09.078
45. Pirhashemi, M.; Habibi-Yangjeh, A. *Ceram. Int.* **2017,** *43,* 13447–13460. doi:10.1016/j.ceramint.2017.07.049
46. Li, S.; Hu, S.; Jiang, W.; Liu, Y.; Liu, J.; Wang, Z. *J. Colloid Interface Sci.* **2017,** *501,* 156–163. doi:10.1016/j.jcis.2017.04.057
47. Li, S.; Hu, S.; Xu, K.; Jiang, W.; Liu, J.; Wang, Z. *Nanomaterials* **2017,** *7,* 22–34. doi:10.3390/nano7010022
48. Li, S.; Hu, S.; Xu, K.; Jiang, W.; Liu, Y.; Leng, Z.; Liu, J. *J. Colloid Interface Sci.* **2017,** *504,* 561–569. doi:10.1016/j.jcis.2017.06.018

49. Zhang, J.; Ma, Z. *J. Taiwan Inst. Chem. Eng.* **2017,** *78,* 212–218. doi:10.1016/j.jtice.2017.06.002
50. Marschall, R. *Adv. Funct. Mater.* **2014,** *24,* 2421–2440. doi:10.1002/adfm.201303214
51. Li, H.; Zhou, Y.; Tu, W.; Ye, J.; Zou, Z. *Adv. Funct. Mater.* **2015,** *25,* 998–1013. doi:10.1002/adfm.201401636
52. Shi, J. *Chem. Rev.* **2013,** *113,* 2139–2181. doi:10.1021/cr3002752

License and Terms